The AAPS Journal, Vol. 16, No. 5, September 2014 (© 2014)
DOI: 10.1208/s12248-014-9628-1

Research Article

An Electrically Tight *In Vitro* Blood–Brain Barrier Model Displays Net Brain-to-Blood Efflux of Substrates for the ABC Transporters, P-gp, Bcrp and Mrp-1

Hans Christian Helms,[1] Maria Hersom,[1] Louise Borella Kuhlmann,[1] Lasina Badolo,[2] Carsten Uhd Nielsen,[1] and Birger Brodin[1,3]

Received 5 May 2014; accepted 28 May 2014; published online 17 June 2014

Abstract. Efflux transporters of the ATP-binding cassette superfamily including breast cancer resistance protein (Bcrp/*Abcg2*), P-glycoprotein (P-gp/*Abcb1*) and multidrug resistance-associated proteins (Mrp's/Abcc's) are expressed in the blood–brain barrier (BBB). The aim of this study was to investigate if a bovine endothelial/rat astrocyte *in vitro* BBB co-culture model displayed polarized transport of known efflux transporter substrates. The co-culture model displayed low mannitol permeabilities of $0.95\pm0.1\cdot10^{-6}$ cm·s^{-1} and high transendothelial electrical resistances of 1,177±101 Ω·cm^2. Bidirectional transport studies with ^{3}H-digoxin, ^{3}H-estrone-3-sulphate and ^{3}H-etoposide revealed polarized transport favouring the brain-to-blood direction for all substrates. Steady state efflux ratios of 2.5±0.2 for digoxin, 4.4±0.5 for estrone-3-sulphate and 2.4±0.1 for etoposide were observed. These were reduced to 1.1±0.08, 1.4±0.2 and 1.5±0.1, by addition of verapamil (digoxin), Ko143 (estrone-3-sulphate) or zosuquidar+reversan (etoposide), respectively. Brain-to-blood permeability of all substrates was investigated in the presence of the efflux transporter inhibitors verapamil, Ko143, zosuquidar, reversan and MK 571 alone or in combinations. Digoxin was mainly transported *via* P-gp, estrone-3-sulphate *via* Bcrp and Mrp's and etoposide *via* P-gp and Mrp's. The expression of P-gp, Bcrp and Mrp-1 was confirmed using immunocytochemistry. The findings indicate that P-gp, Bcrp and at least one isoform of Mrp are functionally expressed in our bovine/rat co-culture model and that the model is suitable for investigations of small molecule transport.

KEY WORDS: blood–brain barrier; breast cancer resistance protein; multidrug resistance-associated protein; p-glycoprotein; polarized small molecule transport.

INTRODUCTION

The blood–brain barrier (BBB) regulates the exchange of molecules between the blood and the brain interstitial fluid. The BBB is impermeable to the majority of drugs and drug candidates, which poses a challenge for the pharmaceutical industry [1]. The brain capillary endothelial cells express complex tight junction networks, which, together with metabolising enzymes and drug transporters, constitute the BBB [2]. A number of transporters of the ATP-binding cassette family, including P-glycoprotein (P-gp/*Abcb1*), breast cancer resistance protein (Bcrp/*Abcg2*) and multidrug resistance-associated proteins (Mrp's/*Abcc*'s), are localized at the luminal membrane of the endothelial cells [3–10], where they restrict access to the central nervous system for a large number of drug compounds [11–14].

Cell culture models can be useful tools to estimate the BBB permeability of new drug candidates *in vitro*, if they display barrier properties comparable to those of the native barrier. Bovine blood–brain barrier *in vitro* models have been studied for more than three decades, and changed culture protocols have gradually improved the models [15]. In primary endothelial monocultures, P-gp activity has previously been demonstrated using uptake and efflux studies in the presence and absence of inhibitors [16–18]. However, these studies did not demonstrate vectorial transport, as the endothelial cells were cultured on culture plates. Other studies have demonstrated expression and function of P-gp in the bovine brain endothelial cells [19–21], but vectorial transport studies have shown efflux ratios below 2 [19–23], which is the generally accepted threshold for concluding active efflux transporter involvement [24]. However, with the exception of the Cecchelli *et al*. [21], these cell culture models displayed transendothelial electrical resistance (TEER) values in the range of 100–300 Ω·cm^2 [20, 22, 23], which are relatively low compared to the estimated *in vivo* barrier TEER of 1,000–2,000 Ω·cm^2 [25, 26].

The apparently low functional expression of P-gp observed in these studies could be due to insufficient differentiation of the endothelial cells into a BBB-like phenotype, or alternatively, an active efflux could have been masked by high paracellular fluxes in the low-resistance monolayers [27–29]. Indeed, one study in a tighter rat triple

[1] Department of Pharmacy, The Faculty of Health and Medical Sciences, University of Copenhagen, Universitetsparken 2, 2100, Copenhagen, Denmark.
[2] H Lundbeck A/S, Discovery DMPK, Valby, Denmark.
[3] To whom correspondence should be addressed. (e-mail: birger.brodin@sund.ku.dk)

co-culture model with TEER ranging from 350–600 $\Omega \cdot cm^2$ and fluorescein permeability of $1.8–4 \cdot 10^{-6}$ $cm \cdot s^{-1}$ resulted in an efflux ratio around 2.5 [30].

Recently, our group published a new culture protocol based on the model published by Gaillard *et al.* [31] to improve the tightness of a bovine endothelium/rat astrocyte BBB model [32, 33]. The co-cultured endothelial cells displayed high TEER values, low mannitol fluxes, and polarized transport of the small molecules, L-glutamate and L-aspartate favouring the abluminal-to-luminal direction [34].

The aim of the present study was to investigate if our bovine endothelial/rat astrocyte *in vitro* BBB co-culture model displayed polarized transport of known efflux transporter substrates. We investigated the tightness of the model during transport experiments, as well as the expression and function of P-gp, Bcrp and Mrp-1 in the model using radiolabelled efflux transporter substrates and immunocytochemistry. Overall, our findings indicate that the endothelial cells of the *in vitro* model functionally express efflux transporters including Bcrp, P-gp and Mrp-1, which mediates a net efflux of transporter substrates from the abluminal to the luminal compartment.

MATERIALS AND METHODS

Materials

The radioisotopes ^{3}H-digoxin (specific activity 40.0 $Ci \cdot mmol^{-1}$), ^{3}H-estrone-3-sulphate (specific activity 54.4 $Ci \cdot mmol^{-1}$) and ^{14}C-D-mannitol (specific activity 58.5 $mCi \cdot mmol^{-1}$) were purchased from Perkin Elmer (Hvidovre, Denmark). ^{3}H-etoposide (specific activity 0.401 $Ci \cdot mmol^{-1}$) was purchased from Moravek Biochemicals (Brea, California, USA). Primary antibodies, mouse α-MRP1 (ab24102), rabbit α-von Willebrand's factor (ab6994), rabbit α-GFAP (ab7260) and rat α-BCRP (ab24115) were from Abcam (Cambridge, United Kingdom), while rabbit α-ABCB1 (PAB11144) was from Abnova (Johngli, Taiwan). Propidium iodide, Alexa-488 conjugated phalloidin and secondary antibodies, goat anti-rabbit IgG and rabbit anti-rat IgG (both coupled to Alexa-488) were from Molecular Probes (Leiden, The Netherlands). All other chemicals and reagents were bought from Sigma-Aldrich (Rødovre, Denmark) unless otherwise stated.

Isolation and Culture of Primary Astrocytes

Astrocytes were isolated according to previously established protocols [35]. After 3 weeks of culture, the astrocytes were passaged, resuspended in DMSO–FBS (1:9) (approximately $2 \cdot 10^6$ cells per vial) and stored in liquid nitrogen. In the third week of culture, the medium was collected. The astrocyte conditioned medium (ACM) was used later during endothelial cell culture.

Isolation of Endothelial Cells and Establishment of Endothelial/Astrocyte Co-cultures

The isolation of bovine brain endothelial cells and the co-culture with astrocytes are described in detail elsewhere [33]. Briefly, brain capillaries were isolated from freshly slaughtered calves below 12 months of age obtained from a slaughterhouse directly after slaughtering (Herlufmagle, Denmark). The grey matter was isolated and homogenized in Dulbecco's Modified Eagles Medium-AQ (DMEM) using a Dounce Tissue Grinder of 40 ml (Wheaton Science Products, Millville, USA). Capillaries were isolated by filtration through 160-μm mesh filters (Millipore, Copenhagen, Denmark) and digested for 1 h in DMEM supplemented with 10% foetal bovine serum, 10 $ml \cdot L^{-1}$ non-essential amino acids (×100) and 100 $U \cdot ml^{-1}$–100 $\mu g \cdot ml^{-1}$ penicillin–streptomycin solution (DMEM-Comp) + enzymes, DNAse I (170 $U \cdot ml^{-1}$), collagenase type III (200 $U \cdot ml^{-1}$) and trypsin TRL (90 $U \cdot ml^{-1}$) (Worthington Biochemical Corporation, Lakewood, USA). The digested suspension was filtered through 200-μm mesh filters (Merrem and La Porte, Zaltbommel, The Netherlands), and the capillary pellet was resuspended in foetal bovine serum–dimethylsulfoxide (9:1) and stored in liquid nitrogen.

Frozen bovine brain capillaries were thawed and cultured for 4 days (37°C, 10% CO_2) in DMEM-Comp–ACM (1:1) supplemented with 125 $\mu g \cdot ml^{-1}$ heparin in collagen type IV/fibronectin (1 $\mu g \cdot cm^{-2}$ of each) coated T75 flasks. The endothelial cells were passaged and seeded at a density of 90,000 $cells \cdot cm^{-2}$ on collagen/fibronectin-coated Transwell polycarbonate filter inserts (area = 1.12 cm^2, pore radius = 0.4 μm, Corning Life Sciences, New York, USA). Astrocytes for direct contact co-culture were prepared 2 days prior to passage of the endothelial cells by turning the filter inserts upside-down and applying cell suspension to the bottom of the inserts (120,000 $cells \cdot cm^{-2}$). The astrocytes were allowed to adhere for 15 min before the inserts were put back in the culture trays. The co-cultures were cultured for three days in DMEM-Comp supplemented with 125 $\mu g\ ml^{-1}$ heparin followed by 3 days of culture in DM+TES consisting of DMEM without $NaHCO_3$ (Gibco, Breda, The Netherlands), supplemented with 8-(4-CPT)-cyclic adenosine monophosphate (312.5 μM), dexamethasone (0.5 μM), RO-20-1724 (17.5 μM) and *N*-[tris(hydroxymethyl)methyl]-2-aminoethanesulfonic acid (TES) (50 mM).

TEER Measurements and Transport Studies

TEER was measured after equilibration to room temperature prior to all experiments, using an Endohm-12 cup electrode chamber (World Precision Instruments, Sarasota, Florida) connected to a Millicell-ERS device (Millipore, Massachusetts, USA).

Transcellular transport studies were performed directly in the culture medium after 6 days of co-culture. 1 $\mu Ci \cdot ml^{-1}$ of the ^{3}H-labelled substrate (either digoxin, estrone-3-sulphate or etoposide) was added to either the luminal or abluminal solution together with 1 $\mu Ci \cdot ml^{-1}$ ^{14}C-D-mannitol. Culture trays were placed on a temperature-controlled shaking table at 37°C, 90 rounds per minute. Aliquots (50 μl from the luminal or 100 μl from the abluminal compartment) were removed from the receiver wells after 30, 60, 90, 120 and 150 min and from the donor wells after 150 min (to confirm mass balance). Samples were replaced with pre-heated (37°C) DM+TES. Samples were transferred to Ultima Gold scintillation fluid (Perkin-Elmer), and radioactivity was counted in a Tri-Carb 2,100 TR Liquid Scintillation Analyzer (Packard Instrument Company, Meriden, USA).

Transport studies were performed in both the luminal-to-abluminal (L–A) and abluminal-to-luminal (A–L) direction. Transporter functionality was evaluated by co-application of the inhibitors, verapamil (50 μM), Ko 143 (0.5 μM) (Toronto Research Chemicals, Toronto, Canada), reversan (5 μM), MK 571 (50 μM), zozuquidar (0.5 μM) and combinations of these. Inhibitors were added to both compartments as ×100 stock solutions 15 min prior to the addition of radiolabelled substrates. Tight junction integrity was assessed by measuring TEER through transport experiments performed without the addition of radiolabelled substrates. TEER was measured at 37°C prior to the experiment as a reference point and subsequently at the time points of sample withdrawal (also at 37°C). An alternative protocol, where the culture medium was changed to Hank's balanced saline solution with calcium/magnesium (HBSS) containing HEPES (10 mM), 0.05% bovine serum albumin (BSA) and the differentiation factors, 8-(4-CPT)-cyclic adenosine monophosphate (312.5 μM), dexamethasone (0.5 μM) and RO-20-1724 (17.5 μM), (same as in the DM+TES culture medium) prior to initiation of the transport experiment was evaluated. The culture medium was replaced with pre-heated HBSS, and the cells were left to equilibrate on the temperature-controlled shaking table for 15 min (37°C, no stirring). Then, the simulated transport experiment was performed as above.

Immunocytochemistry

Cultured cells and freshly isolated capillaries were fixed and permeabilized with 4% paraformaldehyde+0.2% Triton X-100 for 15 min at room temperature and subsequently blocked for 30 min at room temperature in phosphate buffered saline (PBS) supplemented with 2% BSA and 0.1% Tween 20. Samples were stored in PBS+2% BSA and 0.1% Tween 20 or incubated with antibodies against von Willebrand's factor (1:400), glial fibrillary acidic protein (1:500), Bcrp (1:20), P-gp (ABCB1) (1:100) or Mrp1 (1:20) overnight at 4°C. The cells/capillaries incubated with primary antibodies were subsequently incubated 30 min at room temperature with 5 μg ml^{-1} goat anti-mouse IgG (Mrp1), 5 μg ml^{-1} goat anti-rabbit IgG (von Willebrands factor, P-gp, glial fibrillary acidic protein) or 5 μg ml^{-1} rabbit anti-rat IgG (Bcrp), while the cells stored in PBS were incubated 30 min at room temperature with Alexa-488 conjugated phalloidin (1:200). The cells/capillaries were counterstained with propidium iodide (1.5 μM) for 5 min and mounted on coverslips. Cells were imaged using a Zeiss LSM 510 laser confocal microscope (Carl Zeiss, Jena, Germany).

Data Analysis

Measured TEER values were standardized against the surface area of the filter inserts to achieve corrected TEER values as $\Omega \cdot cm^2$. Standardized TEER values measured during transport experiments were plotted against time.

The measured molar amounts in the receiver samples were corrected for the dilution from replacing the receiver samples using Eq. 1:

$$Mass_{total} = V_s \times \left(\sum_{n=1} C_{n-1} \right) + C_n \times V_t \quad (1)$$

V_s is the volume of the receiver samples, V_t is the total volume of the receiver solution and C_n is the concentration of the isotope in the receiver sample, n. The corrected amount transported was plotted as total amount transported per cm^2 per unit of time. Fluxes (J) were calculated from the steady state slopes of the straight lines (accumulated substrate per cm^2 as a function of time). Apparent permeability values were calculated using Eq. 2.

$$P_{app} = \frac{J_{ss}}{C_{donor}} \quad (2)$$

P_{app} is the apparent permeability, J_{ss} is the observed steady-state flux and C_{donor} is the concentration in the donor compartment after spiking. Efflux ratios were calculated as the apparent permeability in the A–L direction divided by the apparent permeability in the L–A direction. Obtained efflux ratios were compared using one-sided analysis of variance (ANOVA) followed by Bonferroni's test (α=0.05).

All curve fitting and statistical analyses were performed in Graph Pad Prism version 6 (GraphPad Software, La Jolla, CA, USA).

Data are reported as means±standard error of the mean (SEM). n denotes the number of times an experiment was performed as a whole. N denotes the number of filter inserts used for each condition within each single experiment.

RESULTS

Bovine Endothelial Cells Co-cultured with Rat Astrocytes Displayed Endothelial Cell Morphology and Expression of von Willebrand's Factor

Bovine brain endothelial cells, co-cultured with rat astrocytes on opposite sides of permeable polycarbonate supports, were characterized using immunocytochemical stainings of filamentous actin and the cell-specific markers for endothelial cells and astrocytes, von Willebrand's factor and glial fibrillary acidic protein, respectively (Fig. 1).

The endothelial cells were large, flat and irregular, with a cobblestone-like morphology as previously observed [33]. The cells were organized in a monolayer, and the filamentous actin was concentrated at the cell borders (Fig. 1a). Von Willebrand's factor was expressed in vesicles throughout the endothelial cells (Fig. 1b). There was no staining of glial fibrillary acidic protein in the endothelial cells, indicating that no astrocytes were present (Fig. 1c). Astrocytes displayed a non-organized layer with irregularly shaped cells (Fig. 1d). No staining of von Willebrand's factor expression was observed (Fig. 1e), whereas glial fibrillary acidic protein was expressed in all astrocytes, although growing cells on top of the astrocyte layer appeared to have the highest expression (Fig. 1f).

The Co-culture Model Displayed High Paracellular Tightness, Which Decreased Gradually During Transport Experiments

The paracellular tightness of the co-culture model was estimated using TEER measurements. On day 6 of co-culture, the TEER (at room temperature) reached an overall

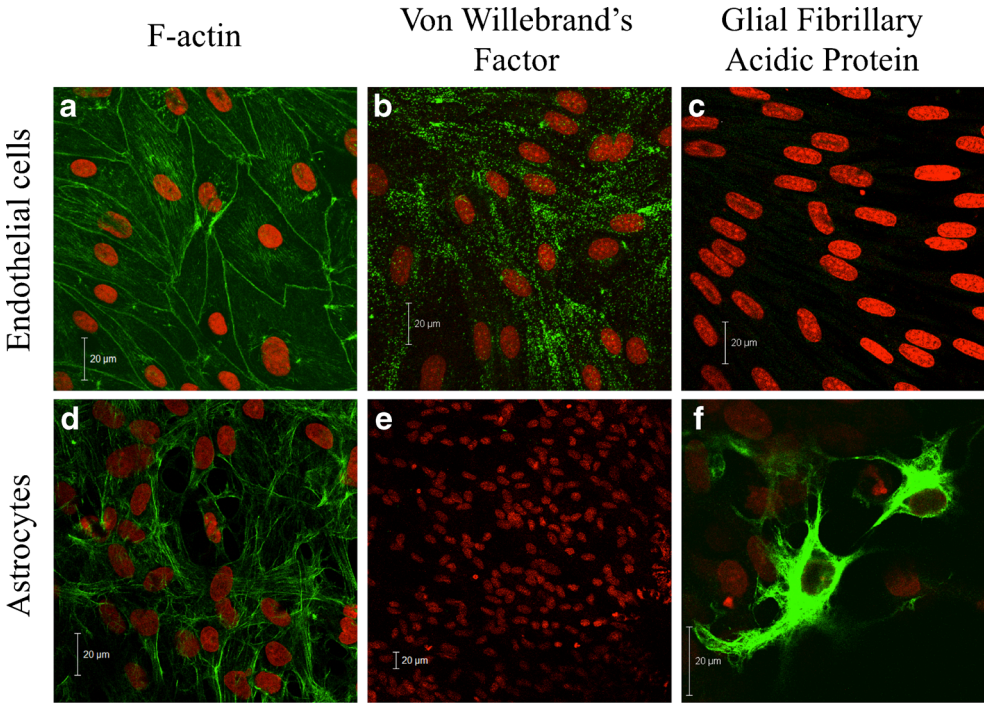

Fig. 1. Immunocytochemical characterization of *in vitro* blood–brain barrier models at day 6 of co-culture. *Upper row* Endothelial cells were stained with Alexa-488 phalloidin to visualize filamentous actin (**a**), with an antibody against von Willebrand's factor (**b**) or an antibody against glial fibrillary acidic protein (**c**) (*green*). Cell nuclei were counterstained with propidium iodide (*red*). *Lower row* Astrocytes stained with Alexa-488 phalloidin (**d**), an antibody against von Willebrand's factor (**e**) or an antibody against glial fibrillary acidic protein (**f**) (*green*). *Bars*=20 µm

average of 1,177±101 $\Omega \cdot cm^2$ (n=31, N=4–18). The TEER of individual batches varied from 327±30 $\Omega \cdot cm^2$ (N=12) to 2,555±399 $\Omega \cdot cm^2$ (N=18).

The change in tightness of the monolayers as a function of experimental time was examined in experiments where co-cultures were placed on a shaking table at 37°C and stirred at 90 rounds per minute. The TEER was measured (at 37°C) at regular intervals, corresponding to the sampling times in a typical transport experiment (Fig. 2).

The resistance of co-cultures, incubated in culture medium, remained stable for the first 60 min after the onset of stirring, followed by a gradual decline from 1,081±31 to 593±68 $\Omega \cdot cm^2$ during the remaining 90 min (n=4). Change of medium from the DM+TES (containing 50 mM TES) to HBSS with 10 mM HEPES, 0.5% BSA and the same differentiation factors as in DM+TES (e.g. RO, cAMP and dexamethasone) caused an immediate drop in resistance to approximately 50% of the initial value followed by a decline during the first 60 min of stirring to approximately 10–20% of the starting level determined in culture media. All subsequent experiments were therefore performed using a protocol where the substrates were added directly to the culture medium.

The transendothelial flux of mannitol was estimated in all transport experiments in the study. The average steady-state mannitol permeability was $0.95 \pm 0.1 \cdot 10^{-6}$ $cm \cdot s^{-1}$ (n=30, N=4–12). Steady-state flux of mannitol was maintained throughout the experiments (data not shown), indicating that the decrease in electrical resistance observed did not increase mannitol transport.

The relationship between the apparent mannitol permeability and the TEER measured prior to the experiment showed a relationship much similar to an exponential decay function (Fig. 3).

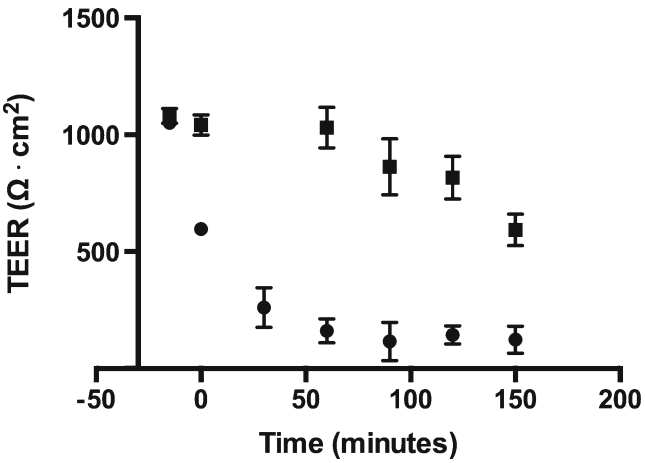

Fig. 2. Change in (TEER of co-cultured monolayers as a function of experimental time. TEER was measured at 37°C to avoid cooling of the cells prior to each measurement. The co-cultures were either incubated with their culture medium (*solid square*) or in HBSS with 10 mM HEPES and 0.5% BSA (*solid circle*). The first data point in both series corresponds to initial TEER-measurement in the culture media at 37°C. The medium was replaced with HBSS in one treatment group after the initial TEER measurement and both groups were incubated 15 min before the onset of stirring. The stirring was started at time zero. Data are averages±SEM (n=3–4, N=2–3)

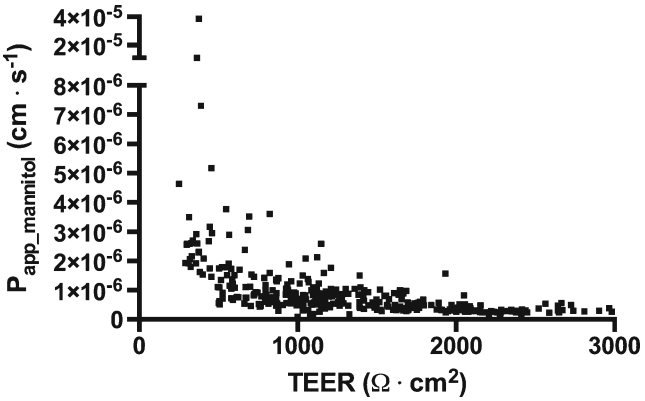

Fig. 3. Mannitol permeability as a function of TEER. Apparent mannitol permeabilities obtained from ^{14}C–D-mannitol (20 μM) flux experiments across single filter inserts plotted as a function of the transendothelial electrical resistance measured across the corresponding filter inserts at room temperature prior to the experiment

The relationship between mannitol permeability and electrical tightness of the cultures indicated that the largest differences in mannitol permeabilities were observed when TEER values were below 500 Ω·cm^2. Increases in TEER above this level only caused small reductions in permeability values (in the ranges between 0.3–1·10^{-6} cm·s^{-1}). This could explain why we observed a decrease in the transendothelial electrical resistance during the last part of the experimental time course (Fig. 2), but not a corresponding increase in mannitol fluxes. However, the variations in mannitol permeabilities were apparently reduced with increasing TEER levels resulting in very low variations when the TEER was above 2,000 Ω·cm^2.

The Efflux Transporter Substrates Digoxin, Estrone-3-Sulphate and Etoposide All Displayed Polarized Transport in the Brain-to-Blood Direction

Efflux transporter activity was examined in bidirectional flux studies. Luminal-to-abluminal (L – A) and abluminal-to-luminal (A – L) transendothelial fluxes of ^{3}H-digoxin (P-gp substrate), ^{3}H-estrone-3-sulphate (Bcrp and Mrp substrate) and ^{3}H-etoposide (P-gp and Mrp substrate) were measured on day 6 of culture (Fig. 4) [36–39].

Transported amount of substrate as a function of time displayed a linear relationship from 30 to 150 min, indicating that the fluxes were in steady-state throughout the transport experiments.

Digoxin displayed steady state permeability values of 2.0±0.2·10^{-6} cm·s^{-1} (L–A) and 4.5±0.3·10^{-6} cm·s^{-1} (A–L), which were changed to 3.5±0.2·10^{-6} cm·s^{-1} (L–A) and 3.2±0.1·10^{-6} cm·s^{-1} (A–L) by co-application of verapamil (Fig. 4a). Estrone-3-sulphate displayed permeability values of 0.62±0.1·10^{-6} cm·s^{-1} (L–A) and 2.2±0.1·10^{-6} cm·s^{-1} (A–L), which were changed to 0.99±0.06·10^{-6} cm·s^{-1} (L–A) and 1.1±0.1·10^{-6} cm·s^{-1} (A–L) by co-application of Ko 143 (Fig. 4b). Etoposide displayed steady-state permeability values of 0.66±0.06·10^{-6} cm·s^{-1} (L–A) and 1.5±0.2·10^{-6} cm·s^{-1} (A–L), which were changed to 0.91±0.07·10^{-6} cm·s^{-1} (L–A) and 1.2±0.1·10^{-6} cm·s^{-1} (A–L) by co-application of zosuquidar and reversan (Fig. 4c). The corresponding efflux ratios are given in Fig. 5.

Digoxin had an efflux ratio of 2.5±0.2 (n=11) indicating a net efflux *via* P-gp from the abluminal to the luminal compartment. Co-administration of 50 μM verapamil caused a significant reduction in the efflux ratio to 1.1±0.08 (n=4) (P=0.0144). Estrone-3-sulphate displayed an efflux ratio of 4.4±0.5 (n=7), indicative of a Bcrp-mediated efflux. The efflux was reduced to 1.4±0.2 (n=3) by co-administration of 0.5 μM Ko 143 (P<0.0001). Etoposide displayed an efflux ratio of 2.4±0.1 (n=4), which was reduced to 1.5±0.1 (n=3) by co-administration of zosuquidar and reversan (P=0.018). For comparison, the efflux ratio of mannitol was 1.2±0.1 (n=25). This was significantly lower than the values observed for digoxin (P<0.0001), estrone-3-sulphate (P<0.0001) and etoposide (P=0.048), whereas it was not significantly different from the efflux ratios in the presence of inhibitors (P=0.70 for digoxin+verapamil, P=0.73 for estrone-3-sulphate+Ko 143, P=0.43 for etoposide+zosuquidar+reversan). The transport studies thus indicated a net "brain-to-blood" (A–L) efflux of all substrates, which was inhibited by co-application of the respective inhibitors.

"Brain-to-blood" transport (A–L) of the three substrates was further examined in the presence of verapamil, Ko 143, zosuquidar, reversan, MK 571 and combinations of those, in order to better discriminate the involvement of the different efflux transporters in the transport process (Fig. 6).

All inhibitors, except Ko 143 and MK 571, significantly inhibited A–L transport of digoxin (P between 0.0019 and

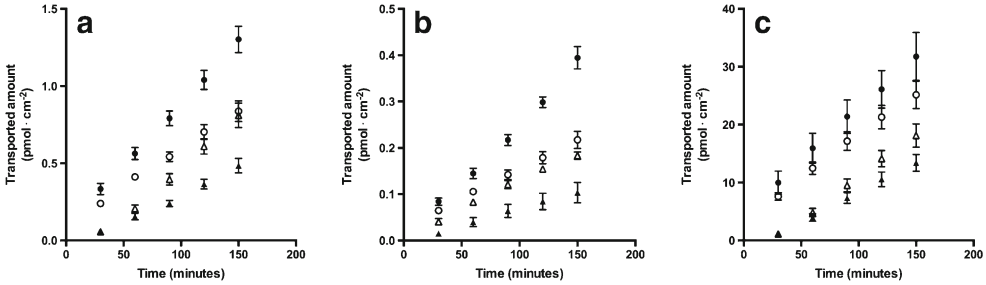

Fig. 4. Transendothelial transport of ^{3}H-digoxin (0.03 μM) (**a**), ^{3}H-estrone-3-sulphate (**b**) (0.02 μM) and ^{3}H-etoposide (**c**) (2.64 μM) across the co-culture model as a function of time, in the luminal-to-abluminal (*solid triangle*) and abluminal-to-luminal direction (*solid circle*) without or with inhibitors (luminal-to-abluminal, *open triangle*; abluminal-to-luminal, *open circle*), verapamil (50 μM) (**a**), Ko 143 (0.5 μM) (**b**) or zosuquidar+reversan (0.5 and 5 μM, respectively) (**c**). Data are means±SEM (n=3–9, N=2–3)

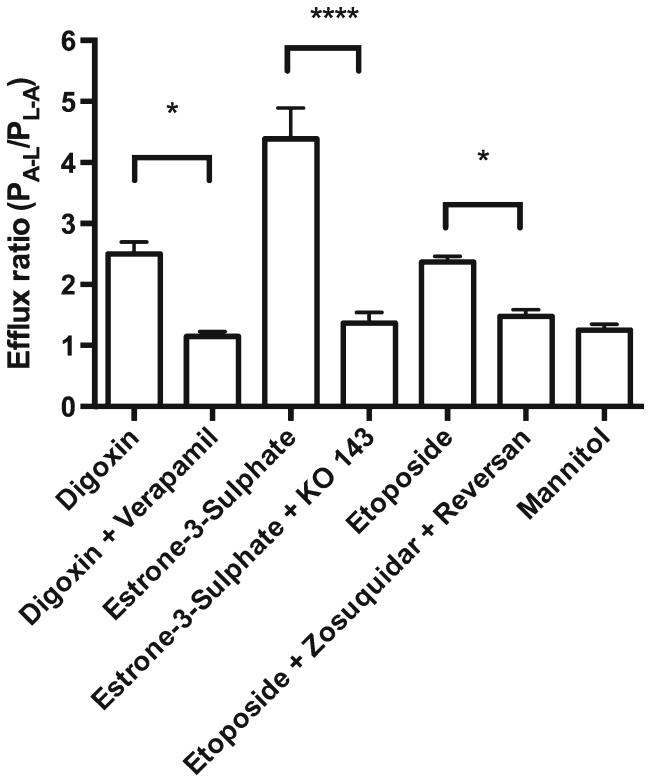

Fig. 5. Efflux ratios derived from the apparent substrate permeabilities. Inhibitors were applied in concentrations of 50 μM (verapamil), 5 μM (reversan) or 0.5 μM (Ko 143 and zosuquidar). Data are means±SEM (n=3–25, N=2–3).*P<0.05, ****P<0.0001

0.009) (Fig. 6a), with no differences between degrees of observed inhibition. This indicated that digoxin was mainly transported *via* P-gp. Estrone-3-sulphate transport was inhibited by all inhibitors (P<0.0001 except for zosuquidar, p=0.0031) (Fig. 6b). This indicated that P-gp, Bcrp and Mrp's were all involved in the transport process, however, to a different degree. Zosuquidar alone had a significantly lower inhibitory effect than all other conditions, indicating that P-gp played a minor role in the transport. The highest degrees of inhibition were observed when Bcrp and Mrp inhibitors were combined, *e.g.* verapamil+Ko 143 or reversan+Ko 143. Ko 143 alone inhibited to a similar degree as MK 571 and reversan alone, indicating similar contributions of Bcrp and Mrp's to the overall A–L transport of estrone-3-sulphate. Zosuquidar, reversan, MK 571 and reversan+zosuquidar all inhibited A–L transport of etoposide (P ranging from 0.0002–0.0045), whereas the other conditions had no significant effects. This indicated that etoposide was mainly transported *via* P-gp and Mrp's, although it was surprising that verapamil did not inhibit the transport (P=0.19).

Taken together, the transport data demonstrate functionally active efflux transporters in the BBB model, with presence of P-gp, Bcrp and at least one isoform of Mrp.

Freshly Isolated Capillaries and Endothelial Cells in Co-culture Expressed P-gp, Bcrp and Mrp-1

The expression of P-gp, Bcrp and Mrp-1 was investigated in freshly isolated bovine brain capillaries and in endothelial cells from co-cultures using immunocytochemistry (Fig. 7).

All three transporters were expressed in brain capillaries (Fig. 7 a–c) as well as in endothelial cells, co-cultured for 6 days (Fig. 7d–i), as judged by immunocytochemical staining. Staining with an antibody against P-gp showed a diffuse expression throughout the cells (Fig. 7d). A similar expression pattern was observed for Mrp-1 (Fig. 7f), whereas Bcrp showed a partial up-concentration at the cell–cell contacts (Fig. 7e). The endothelial cells were further examined from the x,z dimension to determine if the transporters were localized in the luminal membrane (Fig. 7g–i). Low x,z resolution in combination with very thin endothelial cells makes it difficult to determine the exact localization. However, in comparison to the cell nuclei, P-gp expression was seemingly higher at the luminal membrane, whereas Bcrp and Mrp-1 seemed more diffuse.

DISCUSSION

Functional activity of efflux transporters is an important characteristic for *in vitro* BBB models. A recently published retrospective analysis of 32 Pfizer CNS drug candidates led to the conclusion that P-gp/Bcrp affinity was one of the most important factors determining the failure of the candidates [1]. In this study, we evaluated the electrical tightness and

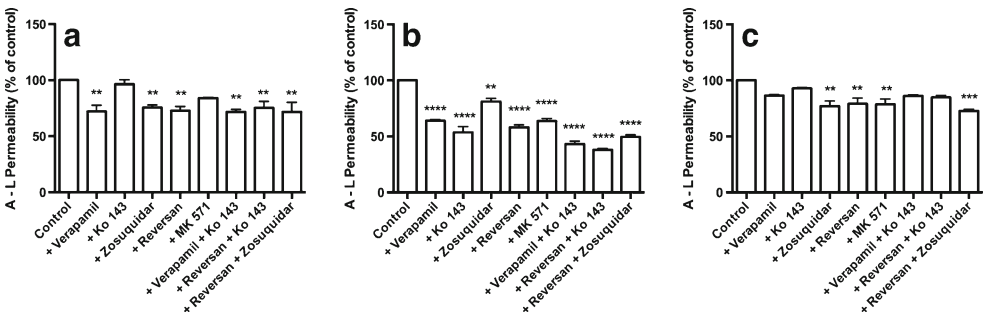

Fig. 6. Abluminal-to-luminal transport of ^{3}H-digoxin (0.03 μM) (**a**), ^{3}H-estrone-3-sulphate (**b**) (0.02 μM) and ^{3}H-etoposide (**c**) (2.64 μM) across the co-culture model in the presence of different inhibitors. Inhibitors were applied in concentrations of 50 μM (verapamil and MK 571), 5 μM (reversan) or 0.5 μM (Ko 143 and zosuquidar). Data are standardized against the substrate permeability without inhibitors performed within the same experiment and shown as means±SEM (n=3–4, N=2–3). **P<0.01, ***P<0.001, ****P<0.0001

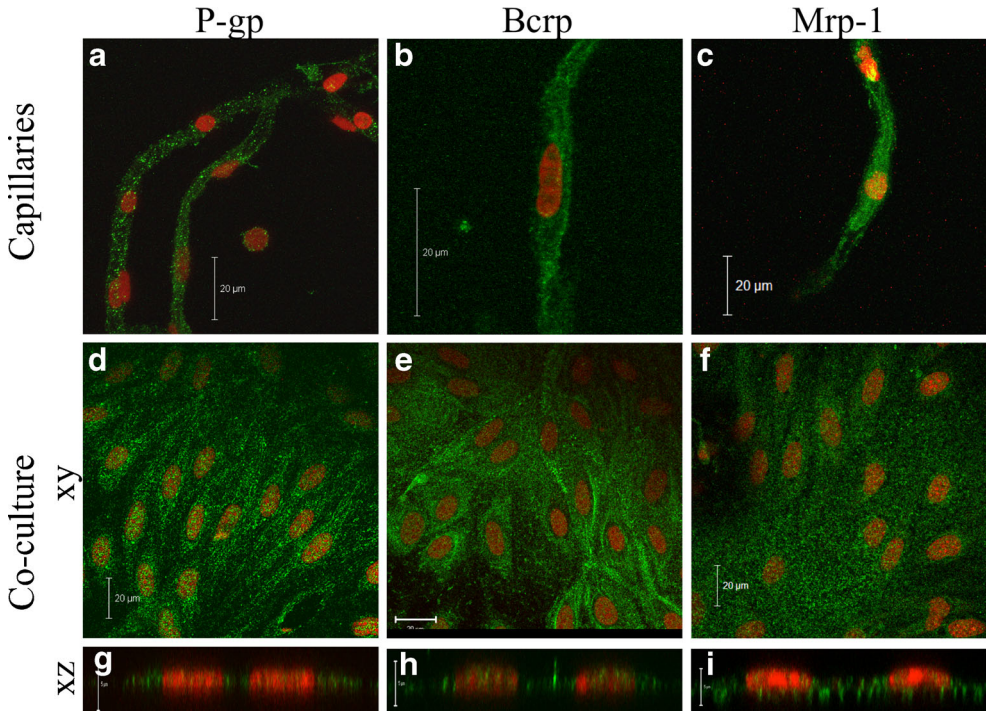

Fig. 7. Immunocytochemical staining of P-glycoprotein (P-gp), breast cancer resistance protein (Bcrp) and multidrug resistance-associated protein-1 (Mrp-1) in bovine brain endothelial cells: Freshly isolated bovine brain capillaries (**a**–**c**) and endothelial cells after 6 days of co-culture (**d**–**i**) were incubated with antibodies against P-glycoprotein (**a**, **d**, **g**), breast cancer resistance protein (**b**, **e**, **h**) or multidrug resistance-associated protein-1 (**c**, **f**, **i**) followed by incubation with species-specific secondary antibodies labelled with Alexa-488 (*green*). All samples were incubated with propidium iodide to visualize cell nuclei (*red*). *Bars*=20 µm (**a**–**f**) or 5 µm (**g**–**i**)

functional expression of P-gp, Bcrp, and Mrp's through determining efflux ratios of three known efflux transporter substrates, digoxin, estrone-3-sulphate and etoposide.

Efflux Transporter Activity in Bovine Blood–Brain Barrier Models

The apparent permeabilities for the three substrates were significantly higher in the A–L than in the L–A direction, which demonstrates that the model has functional efflux transporters and that it is suitable for examination of polarized BBB transport of small molecules. The efflux ratios were all above 2, a value, which has been established as a threshold value for demonstrating the presence of active efflux transporters [24]. The applied substrates and inhibitors were chosen to target P-gp, Bcrp and Mrp's. The ABC transporters have overlapping substrate and inhibitor profiles [40, 41], which makes it difficult to determine the exact contribution of an individual transporter to the efflux of a given substrate in our *in vitro* model. An overview of different studies applying the substrates and inhibitors is given below (Table I).

Digoxin has been widely used as a probe for determining P-gp activity [38]. Brain uptake of digoxin was approximately 35 times larger in P-gp knockout mice as compared to wild-type control mice, which indicated that P-gp is responsible for the low distribution of digoxin to the brain *in vivo* [57]. Digoxin is not a substrate for Bcrp [58], but other studies have indicated that the poor BBB permeability of digoxin is not explained by P-gp alone [11, 38]. Verapamil has been used as a P-gp inhibitor in concentrations from 5 to 150 µM [23, 59–61], but it has also been shown to inhibit Mrp activity in concentrations of 5–10 µM [45, 62] as well as Bcrp activity, although not in the concentration range applied here [63, 64]. In our study, 50 µM verapamil lowered the efflux ratio of digoxin to 1.1, whereas the Bcrp inhibitor, Ko 143, had no effect on the digoxin transport indicating that the verapamil inhibition of A–L digoxin transport we observed was due to inhibition of P-gp or Mrp's. However, the general Mrp-inhibitor MK571 did not inhibit the efflux of digoxin [39, 53, 65]. Zosuquidar, a more specific P-gp inhibitor [37, 51, 65] and reversan, a specific Mrp-1 and P-gp inhibitor [56] and combinations of those both inhibited digoxin transport to the same degree as verapamil. This indicated that the A–L efflux of digoxin was primarily mediated by P-gp in the bovine endothelial cell/rat astrocyte co-culture model.

Estrone-3-sulphate is a substrate for Bcrp [37, 43] and undergoes efflux across the BBB after intra-cerebral injection in rats [36]. Estrone-3-sulphate may be a substrate for other efflux transporters than Bcrp, although zosuquidar (LY335979) did not affect estrone-3-sulphate efflux in Caco-2 cells [37]. The Bcrp inhibitor, Ko 143, was applied to investigate Bcrp involvement in the observed estrone-3-sulphate efflux. Co-administration of 0.5 µM Ko 143 inhibited the estrone-3-sulphate efflux. However, estrone-3-sulphate transport was also affected by co-application of zosuquidar, verapamil, reversan and MK 571. The effect of the most specific P-gp inhibitor, zosuquidar, was low indicating little

Table I. Overview of Applied Substrates and Inhibitors and Their Affinities for P-gp, Bcrp and Mrp's

Compound		Concentration used in this study (μM)	Reported K_m, IC_{50} or K_i (μM)	References
	Substrate of			
Digoxin	P-gp	0.03	P-gp: 170 (K_m)	[42]
Estrone-3-sulphate	Bcrp (Mrp-1)	0.02	Bcrp: 17 (K_m)	[43]
Etoposide	Mrp-1 (P-gp)	2.64	Mrp-1: 255 (K_m)	[44]
	Inhibitor of			
Verapamil	P-gp (Mrp-1, Bcrp)	50	P-gp: 10 (IC_{50}) Mrp-1: 3-5 (IC_{50})	[45–49]
Zosuquidar	P-gp	0.5	P-gp: 0.024–0.07 (IC_{50})	[50, 51]
Ko 143	Bcrp	0.5	Bcrp: 0.01 (IC_{50})	[52]
MK571	Mrp-1/4	50	Mrp-1/4: 5/10 (IC_{50})	[53–55]
Reversan	Mrp-1(P-gp)	5	–	[56]

P-gp involvement in the efflux. Verapamil, reversan and MK 571 inhibited the transport to a similar degree as Ko 143, whereas combinations of Bcrp and Mrp-1 inhibition (e.g. verapamil+Ko 143 and reversan+Ko 143) caused the highest degrees of inhibition. This indicated that both Mrp's and Bcrp are involved in the efflux of estrone-3-sulphate the *in vitro* model. Mrp-1 has previously been shown to transport estrone-3-sulphate, at least in the presence of glutathione [66], and Mrp-1, Mrp-4 and Mrp-5 have been shown at the mRNA transcript level in bovine primary endothelial cell cultures, as well as in the isolated bovine brain capillaries [9].

Etoposide is a known substrate for both P-gp and Mrp-1 [3, 39]. Etoposide displayed active efflux across the BBB model. Zosuquidar, reversan and MK 571 all inhibited the A–L transport of etoposide to some extent, indicating involvement of both Mrp's and P-gp in the efflux of etoposide. Correspondingly, the efflux was fully inhibited by a combination of zosuquidar and reversan. Ko 143 did not inhibit A–L transport confirming that it was a specific Bcrp inhibiter. Verapamil, a combination of Ko 143 and reversan and a combination of Ko 143 and verapamil did not inhibit etoposide A–L transport. This was somewhat surprising, as the applied concentration of verapamil should inhibit P-gp and Mrp's to the same extent as zosuquidar and MK 571/reversan. However, both Mrp-1 and P-gp have multiple binding sites, which could explain distinct effects of the different compounds [39, 67].

The substrate/inhibitor studies indicated expression of both P-gp, Bcrp and at least one isoform of Mrp in the model. Immunocytochemical stainings further confirmed the presence of P-gp, Bcrp and Mrp-1 in the endothelial cells as well as in freshly isolated capillaries. P-gp and Bcrp expression have previously been shown in BBB models [6, 19, 20, 30], whereas Mrp expression is more controversial. Mrp-1 has been shown on the mRNA level in bovine brain capillaries [9] and in bovine and porcine brain endothelial cells [9, 68] and on the protein level in rat brain endothelial cells [30], but also Mrp-4 and -5 mRNA have been shown in bovine and porcine endothelial cells [9, 10, 68]. However, only Mrp-4 was found in a recent human proteomics study on brain capillaries [7]. It is not safe to conclude from these data alone, if our BBB model expresses Mrp-1 or some of the other isoforms. The specificity of the Mrp-1 antibody has not been confirmed against the other isoforms, and the inhibition observed with reversan in the functional studies was generally of the same degree as for zosuquidar. Estrone-3-sulphate transport was inhibited by reversan to a significantly higher degree than by zosuquidar, indicating Mrp-1 expression. However, further studies would have to be performed to clearly distinguish between the Mrp isoforms involved.

Polarized Transport of Efflux Transporter Substrates May Be Difficult to Detect in *In Vitro* Models with Low Paracellular Tightness

A range of bovine-based BBB models have been published through the last 30 years, for review see [15]. The general TEER levels in these models have ranged from approximately 100–800 $\Omega \cdot cm^2$, which is reasonably tight compared to other models. However, we previously demonstrated that TEER across a bovine endothelial/rat astrocyte co-culture BBB model was raised approximately two-fold by culture in highly buffered differentiation medium reaching values above 1,600 $\Omega \cdot cm^2$ [32]. Low TEER in cell culture models may cause lack of polarized transport because of a large paracellular flux contributing to the overall transport of the substrate [28]. A recent study by Hakkarainen *et al.* demonstrated P-gp expression in primary bovine endothelial cells with western blotting and immunofluorescence, as well as P-gp function as evaluated by the calcein-AM assay, but did not observe a net transendothelial P-gp-mediated efflux. The authors also reported low TEER values and high sucrose permeabilities, indicating that the paracellular flux component may have masked the transcellular efflux [20]. We found high TEER values in this study, although they decreased gradually during the transport experiments. This may have been caused by the continuous mechanical stress from stirring and repeated sampling during the experiments, but stirring is important to minimize effects of unstirred water layers within the receiver and donor chambers [28]. However, the fluxes of mannitol remained stable through the experiments in spite of this breakdown, but the partial breakdown may be the reason for our apparent TEER cut-off value of 500 $\Omega \cdot cm^2$, which is higher than previously reported [69]. A method to decrease the apparent decline in paracellular tightness could be to run the experiments directly in the incubator, as shown by Lemmen *et al.* who performed 20-h transport experiments across pig endothelial cells in the incubator with real-time TEER monitoring demonstrating polarized transport of Hoechst dye

and stable TEER values throughout the experiment [70, 71]. This method may not be applicable for short-term transport studies with shaking and frequent sampling, where a gradual decline in TEER can be anticipated. For studies like these, our high-resistance model has demonstrated its usefulness.

Conclusion

The findings in this study indicate that P-gp, Bcrp and at least one isoform of Mrp are expressed and functionally active in the bovine endothelial/rat astrocyte *in vitro* blood–brain barrier co-culture model. Moreover, the model forms high-resistance barriers with low paracellular fluxes of a small hydrophilic compound. The model is therefore a promising tool for investigating BBB permeability and affinity for BBB efflux transporters for small molecular compounds.

REFERENCES

1. Di L, Rong H, Feng B. Demystifying brain penetration in central nervous system drug discovery. Miniperspective. J Med Chem. 2013;56(1):2–12.
2. Abbott NJ, Patabendige AA, Dolman DE, Yusof SR, Begley DJ. Structure and function of the blood–brain barrier. Neurobiol Dis. 2010;37(1):13–25.
3. Sharom FJ. ABC multidrug transporters: structure, function and role in chemoresistance. Pharmacogenomics. 2008;9(1):105–27.
4. Schinkel AH. P-Glycoprotein, a gatekeeper in the blood–brain barrier. Adv Drug Deliv Rev. 1999;36(2–3):179–94.
5. Cordon-Cardo C, O'Brien JP, Casals D, Rittman-Grauer L, Biedler JL, Melamed MR, *et al*. Multidrug-resistance gene (P-glycoprotein) is expressed by endothelial cells at blood–brain barrier sites. Proc Natl Acad Sci U S A. 1989;86(2):695–8.
6. Eisenblatter T, Huwel S, Galla HJ. Characterisation of the brain multidrug resistance protein (BMDP/ABCG2/BCRP) expressed at the blood–brain barrier. Brain Res. 2003;971(2):221–31.
7. Uchida Y, Ohtsuki S, Katsukura Y, Ikeda C, Suzuki T, Kamiie J, *et al*. Quantitative targeted absolute proteomics of human blood–brain barrier transporters and receptors. J Neurochem. 2011;117(2):333–45.
8. Geier EG, Chen EC, Webb A, Papp AC, Yee SW, Sadee W, *et al*. Profiling solute carrier transporters in the human blood–brain barrier. Clin Pharmacol Ther. 2013;94(6):636–9.
9. Zhang Y, Han H, Elmquist WF, Miller DW. Expression of various multidrug resistance-associated protein (MRP) homologues in brain microvessel endothelial cells. Brain Res. 2000;876(1–2):148–53.
10. Leggas M, Adachi M, Scheffer GL, Sun D, Wielinga P, Du G, *et al*. Mrp4 confers resistance to topotecan and protects the brain from chemotherapy. Mol Cell Biol. 2004;24(17):7612–21.
11. Kalvass JC, Maurer TS, Pollack GM. Use of plasma and brain unbound fractions to assess the extent of brain distribution of 34 drugs: comparison of unbound concentration ratios to in vivo p-glycoprotein efflux ratios. Drug Metab Dispos. 2007;35(4):660–6.
12. Nicolazzo JA, Katneni K. Drug transport across the blood–brain barrier and the impact of breast cancer resistance protein (ABCG2). Curr Top Med Chem. 2009;9(2):130–47.
13. Schinkel AH, Smit JJ, van Tellingen O, Beijnen JH, Wagenaar E, van Deemter L, *et al*. Disruption of the mouse mdr1a P-glycoprotein gene leads to a deficiency in the blood–brain barrier and to increased sensitivity to drugs. Cell. 1994;77(4):491–502.
14. Dallas S, Miller DS, Bendayan R. Multidrug resistance-associated proteins: expression and function in the central nervous system. Pharmacol Rev. 2006;58(2):140–61.
15. Abbott NJ, Dolman DM, Yusof S, Reichel A, *et al*. In Vitro Models of CNS Barriers. In: Hammarlund-Udenaes M, de Lange ECM, editors. Drug delivery to the brain. New York: Springer; 2014. p. 163–97.
16. Fontaine M, Elmquist WF, Miller DW. Use of rhodamine 123 to examine the functional activity of P-glycoprotein in primary cultured brain microvessel endothelial cell monolayers. Life Sci. 1996;59(18):1521–31.
17. Lechardeur D, Scherman D. Functional expression of the P-glycoprotein mdr in primary cultures of bovine cerebral capillary endothelial cells. Cell Biol Toxicol. 1995;11(5):283–93.
18. Tsuji A, Terasaki T, Takabatake Y, Tenda Y, Tamai I, Yamashima T, *et al*. P-glycoprotein as the drug efflux pump in primary cultured bovine brain capillary endothelial cells. Life Sci. 1992;51(18):1427–37.
19. Gaillard PJ, van der Sandt IC, Voorwinden LH, Vu D, Nielsen JL, de Boer AG, *et al*. Astrocytes increase the functional expression of P-glycoprotein in an in vitro model of the blood–brain barrier. Pharm Res. 2000;17(10):1198–205.
20. Hakkarainen JJ, Rilla K, Suhonen M, Ruponen M, Forsberg MM. Re-evaluation of the role of P-glycoprotein in in vitro drug permeability studies with the bovine brain microvessel endothelial cells. Xenobiotica; Fate Foreign Compd Biol Syst. 2014;44(3):283–94.
21. Cecchelli R, Dehouck B, Descamps L, Fenart L, Buee-Scherrer VV, Duhem C, *et al*. In vitro model for evaluating drug transport across the blood–brain barrier. Adv Drug Deliv Rev. 1999;36(2–3):165–78.
22. van der Sandt IC, Smolders R, Nabulsi L, Zuideveld KP, de Boer AG, Breimer DD. Active efflux of the 5-HT(1A) receptor agonist flesinoxan *via* P-glycoprotein at the blood–brain barrier. Eur J Pharm Sci. 2001;14(1):81–6.
23. van der Sandt IC, Vos CM, Nabulsi L, Blom-Roosemalen MC, Voorwinden HH, de Boer AG, *et al*. Assessment of active transport of HIV protease inhibitors in various cell lines and the in vitro blood–brain barrier. AIDS. 2001;15(4):483–91.
24. Brouwer KL, Keppler D, Hoffmaster KA, Bow DA, Cheng Y, Lai Y, *et al*. In vitro methods to support transporter evaluation in drug discovery and development. Clin Pharmacol Ther. 2013;94(1):95–112.
25. Crone C, Olesen SP. Electrical resistance of brain microvascular endothelium. Brain Res. 1982;241(1):49–55.
26. Butt AM, Jones HC, Abbott NJ. Electrical resistance across the blood–brain barrier in anaesthetized rats: a developmental study. J Physiol. 1990;429:47–62.
27. Garberg P, Ball M, Borg N, Cecchelli R, Fenart L, Hurst RD, *et al*. In vitro models for the blood–brain barrier. Toxicol In Vitro. 2005;19(3):299–334.
28. Avdeef A. How well can in vitro brain microcapillary endothelial cell models predict rodent in vivo blood–brain barrier permeability? Eur J Pharm Sci. 2011;43(3):109–24.
29. Sjostedt N, Kortejarvi H, Kidron H, Vellonen KS, Urtti A, Yliperttula M. Challenges of using in vitro data for modeling P-glycoprotein efflux in the blood–brain barrier. Pharm Res. 2014;31(1):1–19.
30. Nakagawa S, Deli MA, Kawaguchi H, Shimizudani T, Shimono T, Kittel A, *et al*. A new blood–brain barrier model using primary rat brain endothelial cells, pericytes and astrocytes. Neurochem Int. 2009;54(3–4):253–63.
31. Gaillard PJ, Voorwinden LH, Nielsen JL, Ivanov A, Atsumi R, Engman H, *et al*. Establishment and functional characterization of an in vitro model of the blood–brain barrier, comprising a co-culture of brain capillary endothelial cells and astrocytes. Eur J Pharm Sci. 2001;12(3):215–22.
32. Helms HC, Waagepetersen HS, Nielsen CU, Brodin B. Paracellular tightness and claudin-5 expression is increased in the BCEC/astrocyte blood–brain barrier model by increasing media buffer capacity during growth. AAPS J. 2010;12(4):759–70.
33. Helms HC, Brodin B. Generation of primary cultures of bovine brain endothelial cells and setup of cocultures with rat astrocytes. Methods Mol Biol. 2014;1135:365–82.
34. Helms HC, Madelung R, Waagepetersen HS, Nielsen CU, Brodin B. In vitro evidence for the brain glutamate efflux hypothesis: brain endothelial cells cocultured with astrocytes display a polarized brain-to-blood transport of glutamate. Glia. 2012;60(6):882–93.
35. Hertz L, Juurlink BHJ, Hertz E, Fosmark H. Preparation of primary cultures of mouse (rat) astrocytes. In: Shahar A, Vellis JVAD, Haber B, editors. A dissection and tissue culture manual of the nervous system. New York: Alan R. Liss, Inc; 1989. p. 105-8.

36. Hosoya K, Asaba H, Terasaki T. Brain-to-blood efflux transport of estrone-3-sulfate at the blood–brain barrier in rats. Life Sci. 2000;67(22):2699–711.
37. Xia CQ, Liu N, Yang D, Miwa G, Gan LS. Expression, localization, and functional characteristics of breast cancer resistance protein in Caco-2 cells. Drug Metab Dispos. 2005;33(5):637–43.
38. Ma JD, Tsunoda SM, Bertino Jr JS, Trivedi M, Beale KK, Nafziger AN. Evaluation of in vivo P-glycoprotein phenotyping probes: a need for validation. Clin Pharmacokinet. 2010;49(4):223–37.
39. Cole SP. Targeting multidrug resistance protein 1 (MRP1, ABCC1): past, present, and future. Annu Rev Pharmacol Toxicol. 2014;54:95–117.
40. Matsson P, Englund G, Ahlin G, Bergstrom CA, Norinder U, Artursson P. A global drug inhibition pattern for the human ATP-binding cassette transporter breast cancer resistance protein (ABCG2). J Pharmacol Exp Ther. 2007;323(1):19–30.
41. Matsson P, Pedersen JM, Norinder U, Bergstrom CA, Artursson P. Identification of novel specific and general inhibitors of the three major human ATP-binding cassette transporters P-gp, BCRP and MRP2 among registered drugs. Pharm Res. 2009;26(8):1816–31.
42. Troutman MD, Thakker DR. Efflux ratio cannot assess P-glycoprotein-mediated attenuation of absorptive transport: asymmetric effect of P-glycoprotein on absorptive and secretory transport across Caco-2 cell monolayers. Pharm Res. 2003;20(8):1200–9.
43. Suzuki M, Suzuki H, Sugimoto Y, Sugiyama Y. ABCG2 transports sulfated conjugates of steroids and xenobiotics. J Biol Chem. 2003;278(25):22644–9.
44. Guo A, Marinaro W, Hu P, Sinko PJ. Delineating the contribution of secretory transporters in the efflux of etoposide using Madin-Darby canine kidney (MDCK) cells overexpressing P-glycoprotein (Pgp), multidrug resistance-associated protein (MRP1), and canalicular multispecific organic anion transporter (cMOAT). Drug Metab Dispos. 2002;30(4):457–63.
45. Breuninger LM, Paul S, Gaughan K, Miki T, Chan A, Aaronson SA, *et al.* Expression of multidrug resistance-associated protein in NIH/3T3 cells confers multidrug resistance associated with increased drug efflux and altered intracellular drug distribution. Cancer Res. 1995;55(22):5342–7.
46. Liu WH, Liu HB, Gao DK, Ge GQ, Zhang P, Sun SR, *et al.* ABCG2 protects kidney side population cells from hypoxia/reoxygenation injury through activation of the MEK/ERK pathway. Cell Transplant. 2013;22(10):1859–68.
47. Perrotton T, Trompier D, Chang XB, Di Pietro A, Baubichon-Cortay H. (R)- and (S)-verapamil differentially modulate the multidrug-resistant protein MRP1. J Biol Chem. 2007;282(43):31542–8.
48. Rautio J, Humphreys JE, Webster LO, Balakrishnan A, Keogh JP, Kunta JR, *et al.* In vitro p-glycoprotein inhibition assays for assessment of clinical drug interaction potential of new drug candidates: a recommendation for probe substrates. Drug Metab Dispos. 2006;34(5):786–92.
49. Takara K, Matsubara M, Yamamoto K, Minegaki T, Takegami S, Takahashi M, *et al.* Differential effects of calcium antagonists on ABCG2/BCRP-mediated drug resistance and transport in SN-38-resistant HeLa cells. Mol Med Reports. 2012;5(3):603–9.
50. Choo EF, Leake B, Wandel C, Imamura H, Wood AJ, Wilkinson GR, *et al.* Pharmacological inhibition of P-glycoprotein transport enhances the distribution of HIV-1 protease inhibitors into brain and testes. Drug Metab Dispos. 2000;28(6):655–60.
51. Dantzig AH, Shepard RL, Law KL, Tabas L, Pratt S, Gillespie JS, *et al.* Selectivity of the multidrug resistance modulator, LY335979, for P-glycoprotein and effect on cytochrome P-450 activities. J Pharmacol Exp Ther. 1999;290(2):854–62.
52. Weiss J, Rose J, Storch CH, Ketabi-Kiyanvash N, Sauer A, Haefeli WE, *et al.* Modulation of human BCRP (ABCG2) activity by anti-HIV drugs. J Antimicrob Chemother. 2007;59(2):238–45.
53. Gekeler V, Ise W, Sanders KH, Ulrich WR, Beck J. The leukotriene LTD4 receptor antagonist MK571 specifically modulates MRP associated multidrug resistance. Biochem Biophys Res Commun. 1995;208(1):345–52.
54. Reid G, Wielinga P, Zelcer N, De Haas M, Van Deemter L, Wijnholds J, *et al.* Characterization of the transport of nucleoside analog drugs by the human multidrug resistance proteins MRP4 and MRP5. Mol Pharmacol. 2003;63(5):1094–103.
55. Wortelboer HM, Usta M, van der Velde AE, Boersma MG, Spenkelink B, van Zanden JJ, *et al.* Interplay between MRP inhibition and metabolism of MRP inhibitors: the case of curcumin. Chem Res Toxicol. 2003;16(12):1642–51.
56. Burkhart CA, Watt F, Murray J, Pajic M, Prokvolit A, Xue C, *et al.* Small-molecule multidrug resistance-associated protein 1 inhibitor reversan increases the therapeutic index of chemotherapy in mouse models of neuroblastoma. Cancer Res. 2009;69(16):6573–80.
57. Schinkel AH, Wagenaar E, van Deemter L, Mol CA, Borst P. Absence of the mdr1a P-Glycoprotein in mice affects tissue distribution and pharmacokinetics of dexamethasone, digoxin, and cyclosporin A. J Clin Invest. 1995;96(4):1698–705.
58. Yue W, Abe K, Brouwer KL. Knocking down breast cancer resistance protein (Bcrp) by adenoviral vector-mediated RNA interference (RNAi) in sandwich-cultured rat hepatocytes: a novel tool to assess the contribution of Bcrp to drug biliary excretion. Mol Pharm. 2009;6(1):134–43.
59. Dahan A, Amidon GL. Small intestinal efflux mediated by MRP2 and BCRP shifts sulfasalazine intestinal permeability from high to low, enabling its colonic targeting. Am J Physiol Gastrointest Liver Physiol. 2009;297(2):G371–7.
60. Fenart L, Buee-Scherrer V, Descamps L, Duhem C, Poullain MG, Cecchelli R, *et al.* Inhibition of P-glycoprotein: rapid assessment of its implication in blood–brain barrier integrity and drug transport to the brain by an in vitro model of the blood–brain barrier. Pharm Res. 1998;15(7):993–1000.
61. Luo S, Pal D, Shah SJ, Kwatra D, Paturi KD, Mitra AK. Effect of HEPES buffer on the uptake and transport of P-glycoprotein substrates and large neutral amino acids. Mol Pharm. 2010;7(2):412–20.
62. Abe T, Koike K, Ohga T, Kubo T, Wada M, Kohno K, *et al.* Chemosensitisation of spontaneous multidrug resistance by a 1,4-dihydropyridine analogue and verapamil in human glioma cell lines overexpressing MRP or MDR1. Br J Cancer. 1995;72(2):418–23.
63. Zhang Y, Gupta A, Wang H, Zhou L, Vethanayagam RR, Unadkat JD, *et al.* BCRP transports dipyridamole and is inhibited by calcium channel blockers. Pharm Res. 2005;22(12):2023–34.
64. Maliepaard M, van Gastelen MA, Tohgo A, Hausheer FH, van Waardenburg RC, de Jong LA, *et al.* Circumvention of breast cancer resistance protein (BCRP)-mediated resistance to camptothecins in vitro using non-substrate drugs or the BCRP inhibitor GF120918. Clin Cancer Res. 2001;7(4):935–41.
65. Mease K, Sane R, Podila L, Taub ME. Differential selectivity of efflux transporter inhibitors in Caco-2 and MDCK-MDR1 monolayers: a strategy to assess the interaction of a new chemical entity with P-gp, BCRP, and MRP2. J Pharm Sci. 2012;101(5):1888–97.
66. Qian YM, Song WC, Cui H, Cole SP, Deeley RG. Glutathione stimulates sulfated estrogen transport by multidrug resistance protein 1. J Biol Chem. 2001;276(9):6404–11.
67. Dey S, Ramachandra M, Pastan I, Gottesman MM, Ambudkar SV. Evidence for two nonidentical drug-interaction sites in the human P-glycoprotein. Proc Natl Acad Sci U S A. 1997;94(20):10594–9.
68. Zhang Y, Li CS, Ye Y, Johnson K, Poe J, Johnson S, *et al.* Porcine brain microvessel endothelial cells as an in vitro model to predict in vivo blood–brain barrier permeability. Drug Metab Dispos. 2006;34(11):1935–43.
69. Gaillard PJ, de Boer AG. Relationship between permeability status of the blood–brain barrier and in vitro permeability coefficient of a drug. Eur J Pharm Sci. 2000;12(2):95–102.
70. Lemmen J, Tozakidis IE, Bele P, Galla HJ. Constitutive androstane receptor upregulates Abcb1 and Abcg2 at the blood–brain barrier after CITCO activation. Brain Res. 2013;1501:68–80.
71. Lemmen J, Tozakidis IE, Galla HJ. Pregnane X receptor upregulates ABC-transporter Abcg2 and Abcb1 at the blood–brain barrier. Brain Res. 2013;1491:1–13.